Hindawi Publishing Corporation
International Journal of Photoenergy
Volume 2013, Article ID 394079, 7 pages
http://dx.doi.org/10.1155/2013/394079

Research Article

CTAB-Assisted Hydrothermal Synthesis of $Bi_2Sn_2O_7$ Photocatalyst and Its Highly Efficient Degradation of Organic Dye under Visible-Light Irradiation

Weicheng Xu,[1] Zhang Liu,[1] Jianzhang Fang,[1] Guangyin Zhou,[1] Xiaoting Hong,[1] Shuxing Wu,[1] Ximiao Zhu,[1] YunFang Chen,[1] and Chaoping Cen[2]

[1] *College of Chemistry and Environment, South China Normal University, Guangzhou 510631, China*
[2] *The Key Laboratory of Water and Air Pollution Control of Guangdong Province, South China Institute of Environmental Sciences, Guangzhou 510655, China*

Correspondence should be addressed to Jianzhang Fang; fangjzh@scnu.edu.cn

Received 24 May 2013; Accepted 3 July 2013

Academic Editor: Jiaguo Yu

Pyrochlore-type $Bi_2Sn_2O_7$ (BSO) nanoparticles have been prepared by a hydrothermal method assisted with a cationic surfactant cetyltrimethylammonium bromide (CTAB). These BSO products were characterized by powder X-ray diffraction (XRD), infrared spectroscopy (IR), scanning electron microscopy (SEM), transmission electron microscopy (TEM), Brunauer-Emmett-Teller (BET), and UV-visible diffuse reflectance spectroscopy (DRS). The results indicated that CTAB alters the surface parameters and the morphology and enhances the photoinduced charge separation rate of BSO. The photocatalytic degradation test using rhodamine B as a model pollutant showed that the photocatalytic activity of the BSO assisted with CTAB was two times that of the reference BSO. Close investigation revealed that the size, the band gap, the structure, and the existence of impurity level played an important role in the photocatalytic activities.

1. Introduction

Synthetic textile dyes and other industrial dyestuffs are important organic pollutants and produced all over the world. Their release as wastewater in the ecosystem will cause serious consequences, such as esthetic pollution, eutrophication, and perturbations in aquatic life [1, 2]. Many treatments have been developed and photocatalytic oxidation is regarded as a "green" technology for the decomposition of the soluble dyes in wastewater [3]. Nanosized TiO_2 semiconductor has been considered as one of the most promising photocatalysts in practical applications due to its high photocatalytic activity, chemical stability, low cost, and nontoxicity [4, 5]. However, the TiO_2 photocatalyst has no visible-light response due to its large band gap of 3.2 eV [6]. As a result, there are two strategies to develop the visible-light-driven photocatalysts: modification of TiO_2 [7–11] and exploitation of novel semiconductor materials [12–15]. Recently, many investigations have been undertaken on the latter strategy. A great deal of effort has been devoted to developing photocatalysts containing bismuth with high activities for environmental applications and/or water splitting, such as α-Bi_2O_3 [14], Bi_2WO_6 [15], $BiVO_4$ [12], $CaBi_2O_4$ [16] and $Bi_2O_2CO_3$ [17]. Zhou et al. [7] have synthesized mesoporous Au-TiO2 nanocomposite with high visible-light photocatalytic activity. Chen et al. [6] reported that some dyes could be degraded under visible-light irradiation over TiO2 by a self-photosensitized process. However, its photoefficiency was rather low due to the much slower interfacial electron transfer to the oxidize sensitizer. Therefore, the development of efficient visible-light-induced bismuth-based oxides photocatalysts through new synthetic routes has been an urgent issue.

$Bi_2Sn_2O_7$, a novel important semiconducting material with a typical pyrochlore structure and a band gap of 2.88 eV [18], has received considerable attention in catalysis and gas sensors [19–23]. However, the photocatalytic performance of bismuth stannate should be further improved for practical use. In order to overcome the defect, some researches have

shown that properties of the matter were limited by its size, shape, and specific surface area. Therefore, recently, in order to explore some photocatalysts with specific morphologies and unique properties, surfactant containing system has been employed to the preparation of nanosized photocatalysts. Liu et al. achieved nanocrystalline TiO_2 in microemulsions by using CTAB as surfactant [24]. Yin et al. have synthetized highly efficient monoclinic $BiVO_4$ with the assistance of CTAB [25]. Shen et al. found that the photocatalytic activities of $ZnIn_2S_4$ photocatalysts improved with the amounts of CTAB increasing [26]. CTAB can make the surface of photocatalysts hydrophobic, which is beneficial to the adsorption of nonionic organic compounds onto the photocatalyst and will improve the photocatalytic efficiency. Moreover, synthetic method also played an important role in preparing samples. Solid-state reaction technique had been a common method for the synthesis of pyrochlore BSO [12, 16, 17]. Compared with solid-state reaction, hydrothermal route [18] provided a milder environment for the pyrochlore BSO and the reaction parameters could be easily tuned. However, to the best of our knowledge, the synthesis of BSO by hydrothermal method with surfactant CTAB as the template has not been reported.

In this paper, we developed a facile surfactant (CTAB)-assisted hydrothermal method to prepare BSO photocatalyst at 180°C and the sample was labeled as C-BSO. A model dye of rhodamine B (RhB) was used to evaluate its photocatalytic efficiency under visible-light irradiation. Furthermore, the effects of CTAB on the crystal structure, morphology, and photocatalytic activity were discussed in detail.

2. Experimental

2.1. Synthesis. All the reagents were of analytical purity and used without further purification. In a typical reaction, $K_2SnO_3{\cdot}3H_2O$ (3 mmol) and $Bi(NO_3)_3{\cdot}5H_2O$ (3 mmol) were added by stoichiometric ratio, and 0.3 mmol CTAB was dissolved in a Teflon liner with 100 mL capacity containing 80 mL of deionized water. Under vigorous stirring, the pH value of the mixture was adjusted to 12 by using 2 mol/L KOH, and then the Teflon liner was sealed in the stainless steel autoclave and maintained at 180°C for 24 h. The as-prepared products were obtained by filtration and washed with deionized water and absolute ethanol several times. Finally, the products were dried in hot air oven at 80°C for 12 h. BSO was also prepared by the same procedure mentioned previously without the presence of CTAB.

2.2. Characterization. Samples were characterized by using X-ray diffraction (XRD) with a Bruker D8 Advance diffractometer using Cu KR (λ = 1.5406 nm) and operating at 40 kV and 40 mA. FT-IR spectra were taken in a Shimadzu IR Prestige-21 Fourier transform spectrometer. A scanning electron microscopy (SEM) images were obtained on a JEOL JSM-6700F instrument. Transmission electron microscopy (TEM) images were obtained with a JEOL JEM-2100HR field-emission electron microscope. The Brunauer-Emmett-Teller (BET) specific surface areas of the materials were detected by Micromeritics ASAP 2010 nitrogen adsorption apparatus. UV-visible absorption spectra of the samples were determined on a Hitachi U-3010 UV-Vis spectrophotometer with $BaSO_4$ as the reference.

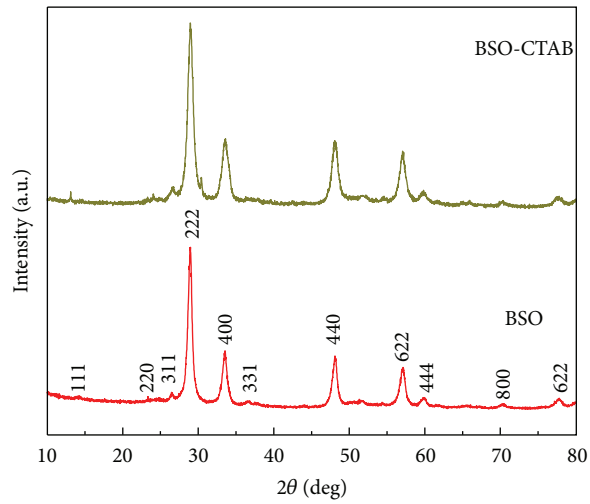

Figure 1: XRD patterns of BSO and C-BSO photocatalysts.

2.3. Photocatalytic Test. The photocatalytic efficiencies of BSO were evaluated by the degradation of RhB under visible-light irradiation. A 300 W Xe arc lamp (LTIC 300BF, Boyi Ltd, China) was used as the light source with a 420 nm cutoff filter. In every experiment, 0.1 g of catalyst was immersed in a 250 mL Pyrex beaker with 100 mL of RhB solution (5 mg/L). In order to ensure adsorption/desorption equilibrium between RhB and the photocatalyst, the suspension was stirred in the dark for 1 h. As for the photocatalytic reactions, 3 mL of the suspensions was taken out at given time intervals and centrifuged to remove the photocatalyst particles. The concentrations of the centrifuged RhB solutions were monitored using a UV-Vis 8500 spectrophoto-meter (Shanghai Tianmei Science Apparatus Ltd. Co. China).

3. Results and Discussion

3.1. Structural and Morphological Characterization. The XRD patterns of as-prepared samples are shown in Figure 1. All strong peaks can be indexed to a pure cubic phase of BSO (JCPDS no. 87-0284). No other peaks can be observed, indicating high purity of the final products. The average sizes of the crystallite estimated using the Scherrer equation from (222) crystal plane of pyrochlore phase at $2\theta = 28.8°$ are 13.5 and 10.2 nm for BSO and C-BSO, respectively. Compared with the BSO sample, the diffraction peak intensity of the C-BSO nanoparticles is weak and broad. This implies that the crystallite size of C-BSO catalyst is smaller than that of the BSO catalyst.

The IR spectrum of the BSO and C-BSO samples, recorded in the range 400–4000 cm^{-1}, is shown in Figure 2. Subramanian et al. have reported the infrared spectra of the pyrochlore oxides and demonstrated that the band at about 600 cm^{-1} was from the B-O stretching vibration in the BO_6

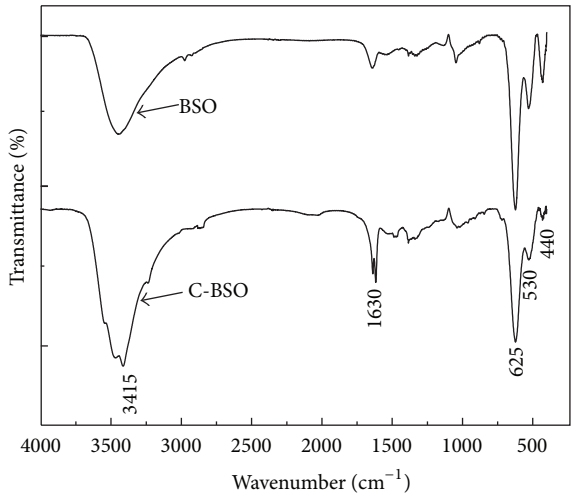

Figure 2: IR spectrum of the as-prepared BSO and C-BSO samples.

octahedron and the A-O stretching vibration of pyrochlore $A_2B_2O_7$ centered at about 500 cm^{-1} [27]. Similar results are obtained by the previous present work. It can be seen clearly that the main band at about 625 cm^{-1} is assigned to the Sn-O stretching vibration while the weak bands of 440 cm^{-1} and 530 cm^{-1} are ascribed to Bi-O-Bi bonds vibrations [28]. The bands centered at about 3415 cm^{-1} and 1630 cm^{-1} are assigned to O-H stretching and bending modes of water, respectively [29].

The morphology of BSO and C-BSO is characterized by SEM as shown in Figure 3. Figure 3(a) shows the BSO samples which consist of a large number of microspheres, indicating that highyield of products can be readily achieved through this approach. Figure 3(b) shows the SEM image of the C-BSO photocatalyst; it can be seen that the irregular lumps and particles are relatively dispersed. The size of the as-prepared BSO nanoparticles is in the range of 8–20 nm (Figure 3(a)). After modification by CTAB, the size of the C-BSO sample has slightly changed. The mean mesopore size is about 10–15 nm, which is consistent with the pore size calculated from N2 isotherms.

The high-magnification TEM images of the BSO and C-BSO samples are shown in Figure 4. Figure 4(a) displays various specifications block-like morphology with sizes of 8–20 nm. Figure 4(b) shows irregular spherical-like morphology of C-BSO, and the sizes of C-BSO are only slightly smaller than BSO sample. Clearly, the size of the as-synthesized C-BSO is smaller than BSO. This phenomenon is consistent with the typical crystallite sizes calculated from XRD results.

3.2. N_2 Adsorption/Desorption Isotherm Analysis. The N_2 adsorption-desorption isotherms and pore size distributions of BSO and C-BSO are determined by BET and BJH methods (shown in Figure 5). The isotherms of all the two samples are of classical type IV, characteristic of mesoporous materials according to the IUPAC. The result indicates that the BET surface area of nanosized BSO samples increased, from 45.3 to 71.9 m^2/g, accompanied with the increase of pore volumes from 0.11 to 0.18 m^2/g. The pore size distribution curves of BSO and C-BSO determined by BJH method from the absorption branch of the isotherms exhibit one single narrow peak centered at 12.7 nm, indicating the good homogeneity of the pores.

3.3. UV-Vis Diffuse Reflectance Spectra. Figure 6 shows the diffuse reflectance spectra of the BSO and C-BSO samples. It is clearly visible from the spectra that the absorption edge of C-BSO gets further shifted to the visible region comparing to the BSO sample. The band gap absorption edges of the BSO and C-BSO are measured to be 450 nm (2.76 eV) and 464 nm (2.67 eV), respectively. Such differences may be ascribed to the changes of crystallite phase and the size of coupled oxides, defects, and so on [30]. In this work, we believe that C-BSO photocatalyst, with its long wavelength absorption band, is an attractive photocatalyst for pollutant. The narrower band gap of C-BSO photocatalyst not only benefits the absorption of more photons in sunlight, but also promotes the excitation of photogenerated electrons from the valence band (VB) to the conduction band (CB), which may make the photocatalyst with high photocatalytic activity.

3.4. Photocatalytic Activity of BSO and C-BSO Nanocomposites under Visible Conditions. The photocatalytic performance of BSO and C-BSO is compared and presented in Figure 7, where C and C_0 represent the time-dependent concentration and the initial concentration of pollutants solution, respectively. The blank test exhibits extremely low photodegradation efficiency in the absence of a photocatalyst under visible-light irradiation. The decrease of RhB concentration in the presence of BSO under visible light is about 51.0% after six hours of illumination. It can be found that the photodegradation efficiency of BSO assisted with CTAB decreases with the increase of CTAB amounts. However, their photocatalytic efficiency can be significantly improved compared with the sample without CTAB. 0.3 mmol C-BSO product exhibits better photodegradation activity than 1.5 mmol C-BSO photocatalyst, with the RhB concentration reduced as much as 97.8% under the same condition.

3.5. Effect of CTAB Assistance. As an efficient sorbent material, supramolecular assemblies (hemimicelles/admicelles) are formed from adsorption of surfactants on the surface of metal oxides. Attractive electrostatic interactions between the head group of ionic surfactants and oppositely charged groups on the oxide lead to the formation of monolayers of adsorbed surfactant termed hemimicelles. After saturation of the oxide surface, hydrophobic interactions between hydrocarbon chains of surfactant molecules lead to the formation of admicelles [31]. In term of hemimicelles, the hydrophobic tails are exposed to aqueous solution, so that the surfactant-coated oxide surface will become hydrophobic, which contributes to the adsorption of nonionic organic compounds onto the adsorbents [32]. Owing to the possession of higher special areas and more ion-exchangeable OH groups on surface, BSO materials have obvious advantage for the sorption

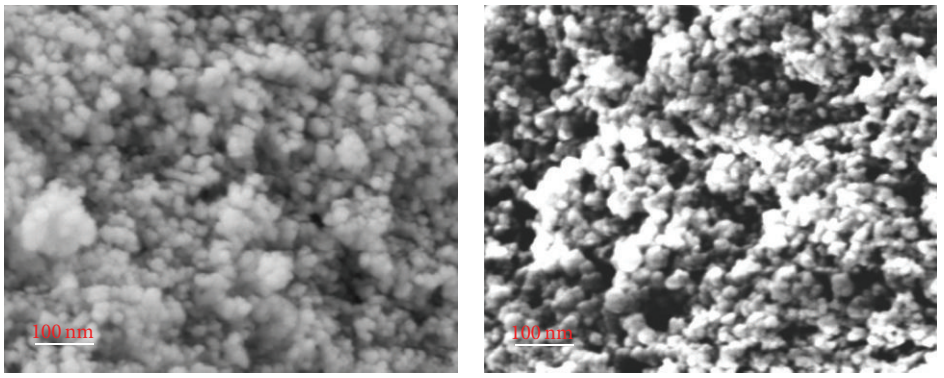

(a) (b)

Figure 3: SEM images of as-prepared samples, (a) BSO sample and (b) C-BSO sample.

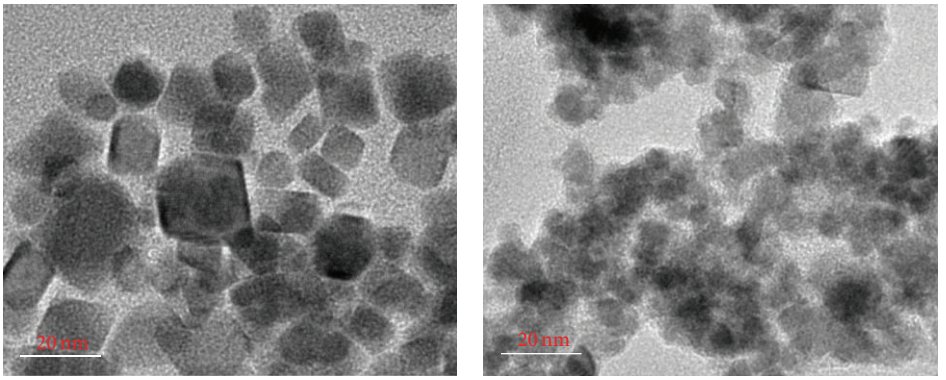

(a) (b)

Figure 4: TEM images of (a) BSO sample and (b) C-BSO sample.

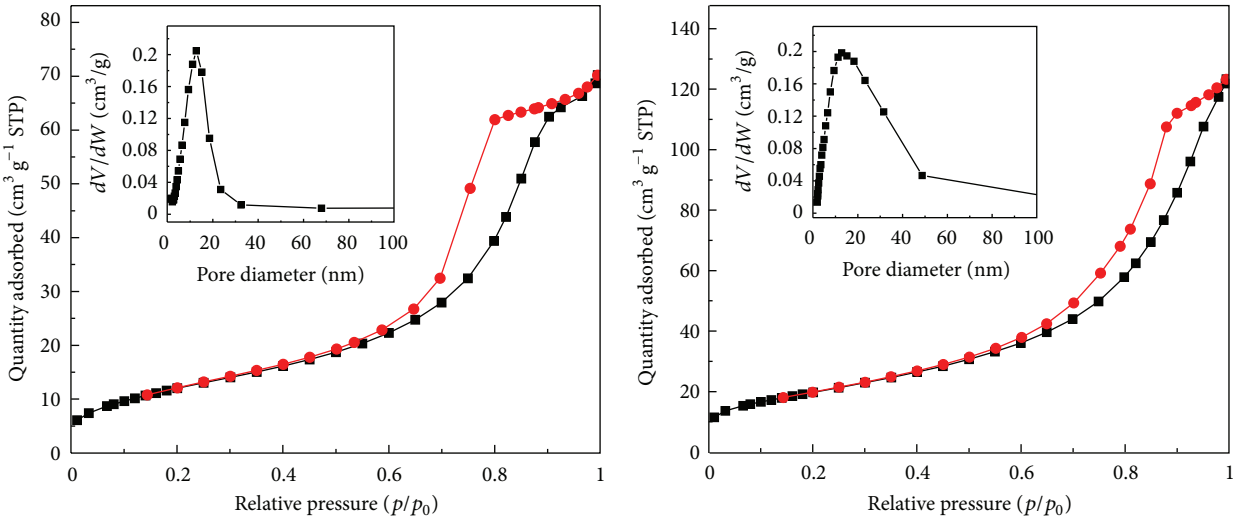

(a) (b)

Figure 5: The N_2 sorption isotherms and pore width distribution of as-synthesized samples and (a) BSO, (b) C-BSO sample.

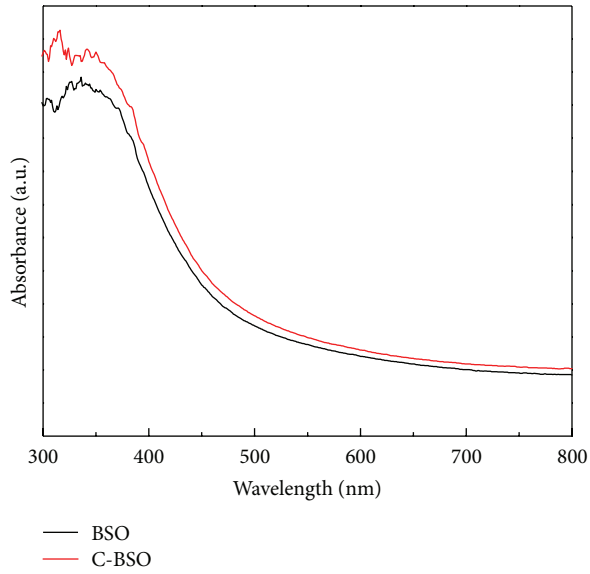

Figure 6: UV-Vis diffuse reflectance spectra of BSO and C-BSO samples.

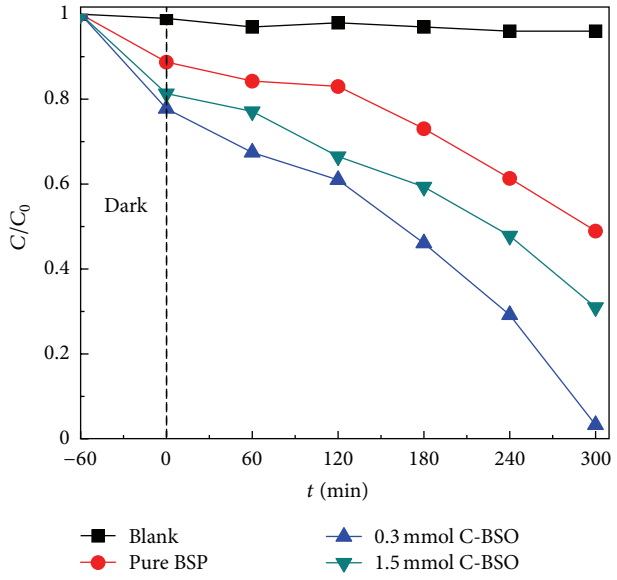

Figure 7: Degradation curves of RhB over as-prepared nanoparticles.

of ionic surfactant and have remarkable adsorption capability to organic compounds correspondingly [33]. Therefore, as shown in Figure 7, the nanomaterials BSO prepared by using CTAB are advantageous in photocatalytic reaction.

3.6. Reasons for Enhanced Efficiency of Photocatalysts. The photocatalytic activity of pyrochlore BSO is strongly influenced by its phase structure, crystallite size, and specific surface area [25]. From the XRD results, the phase structure of BSO did not change before and after using CTAB and retained the good crystallization. The crystallite size of BSO decreased from 13.5 nm to 10.2 nm after using CTAB, which

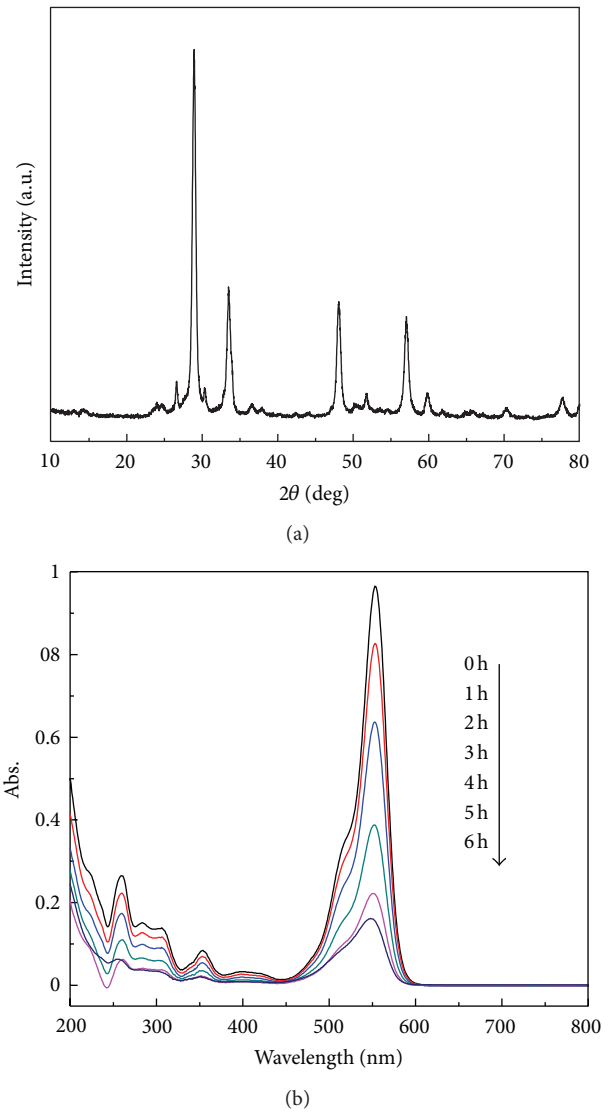

Figure 8: (a) XRD patterns of C-BSO-cal; (b) photocatalytic activities of RhB of C-BSO-cal product.

may be good for the enhancement of their photocatalytic performance. Moreover, the sample prepared with CTAB exhibited larger surface area (71.9 m^2/g) than the reference BSO (45.3 m^2/g). As the specific surface area and pore volume increased, it could result in the transition of band electron indirectly and the enhancement of the generation rate of photogenerated carriers [34]. Therefore, it also can be concluded that the surface area and pore structure of this sample played an important role in its degradation efficiency for wastewater. Moreover, another factor may be the existence of impurity level which could give rise to the shift of absorption edge to the long wavelength side and thus improves photocatalytic efficiency.

In order to test the previous assertion, the C-BSO is calcined at 600°C for 2 h to remove the impurity level (labelled as C-BSO-cal). The XRD pattern of C-BSO-cal (Figure 8(a)) reveals that the C-BSO-cal has the same phase as the C-BSO. The BET surface area of the C-BSO-cal is much smaller

than that of the C-BSO, which can respond for the decline of photocatalytic efficiency of the C-BSO-cal. The photocatalytic efficiency of the C-BSO-cal is presented in Figure 8(b). Obviously, only about 85.1% of RhB is degraded after 6 h of irradiation. It can be attributed to the elimination of impurity level by calcination that affects the removal efficiency of RhB.

4. Conclusions

In conclusion, nanoscale BSO could be conveniently synthesized by a CTAB assisted hydrothermal process at the temperature 180°C for 24 h. The experimental results show that adding CTAB into the synthesis system resulted in excellent dispersivity of lumps blocks and particles spheres with irregular shapes. BET surface area and pore volume of C-BSO are higher than those of BSO sample. Moreover, the photocatalytic activity of C-BSO is two times that of the reference BSO. The results demonstrate that the excellent photocatalytic activity of C-BSO stems from the efficiency of electron-hole pairs separation rate and the existence of impurity levels in C-BSO crystals.

Acknowledgment

This work was supported by Guangdong Water and Air Pollution Control Key Laboratory (2011 A060901002) open funded project.

References

[1] M. A. Brown and S. C. deVito, "Predicting azo dye toxicity," *Critical Reviews in Environmental Science and Technology*, vol. 23, no. 3, pp. 249–324, 1993.

[2] N. Z. Bao, X. Feng, Z. H. Yang, L. Shen, and X. Lu, "Highly efficient liquid-phase photooxidation of an azo dye methyl orange over novel nanostructured porous titanate-based fiber of self-supported radially aligned $H_2Ti_8O_{17}\cdot 1.5H_2O$ nanorods," *Environmental Science and Technology*, vol. 38, no. 9, pp. 2729–2736, 2004.

[3] J. Bi, L. Wu, J. Li, Z. Li, X. Wang, and X. Fu, "Simple solvothermal routes to synthesize nanocrystalline Bi_2MoO_6 photocatalysts with different morphologies," *Acta Materialia*, vol. 55, no. 14, pp. 4699–4705, 2007.

[4] L. Zhao, J. R. Ran, Z. Shu, G. Dai, P. Zhai, and S. Wang, "Effects of calcination temperatures on photocatalytic activity of ordered titanate nanoribbon/SnO_2 films fabricated during an EPD process," *International Journal of Photoenergy*, vol. 2012, Article ID 472958, 7 pages, 2012.

[5] G. F. Shang, H. B. Fu, S. Yang, and T. Xu, "Mechanistic study of visible-light-induced photodegradation of 4-chlorophenol by $TiO_{2-x}N_x$ with low nitrogen concentration," *International Journal of Photoenergy*, vol. 2012, Article ID 759306, 9 pages, 2012.

[6] C. C. Chen, W. Zhao, J. Y. Li, J. Zhao, H. Hidaka, and N. Serpone, "Formation and identification of intermediates in the visible-light-assisted photodegradation of sulforhodamine-B dye in aqueous TiO_2 dispersion," *Environmental Science and Technology*, vol. 36, no. 16, pp. 3604–3611, 2002.

[7] P. Zhou, J. G. Yu, and Y. X. Wang, "The new understanding on photocatalytic mechanism of visible-light response N-S codoped anatase TiO_2 by first-principles," *Applied Catalysis B*, vol. 142-143, pp. 45–53, 2013.

[8] R. Asahi, T. Morikawa, T. Ohwaki, K. Aoki, and Y. Taga, "Visible-light photocatalysis in nitrogen-doped titanium oxides," *Science*, vol. 293, no. 5528, pp. 269–271, 2001.

[9] J. G. Yu, G. P. Dai, Q. Xiang, and M. Jaroniec, "Fabrication and enhanced visible-light photocatalytic activity of carbon self-doped TiO_2 sheets with exposed 001 facets," *Journal of Materials Chemistry*, vol. 21, no. 4, pp. 1049–1057, 2011.

[10] M. H. Zhou, J. Zhang, B. Cheng, and H. G. Yu, "Enhancement of visible-light photocatalytic activity of mesoporous Au-TiO_2 nanocomposites by surface plasmon resonance," *International Journal of Photoenergy*, vol. 2012, Article ID 532843, 10 pages, 2012.

[11] R. Liu,, P. Wang, X. Wang, H. Yu, and J. Yu, "UV-and visible-light photocatalytic activity of simultaneously deposited and doped Ag/Ag(I)-TiO_2 photocatalyst," *Journal of Physical Chemistry C*, vol. 116, no. 33, pp. 17721–17728, 2012.

[12] M. Long, W. Cai, J. Cai, B. Zhou, X. Chai, and Y. Wu, "Efficient photocatalytic degradation of phenol over Co_3O_4/$BiVO_4$ composite under visible light irradiation," *Journal of Physical Chemistry B*, vol. 110, no. 41, pp. 20211–20216, 2006.

[13] Q. Li, H. Meng, P. Zhou et al., "$Zn_{1-x}Cd_xS$ solid solutions with controlled bandgap and enhanced visible-light photocatalytic H_2-production activity," *ACS Catalysis*, vol. 3, no. 5, pp. 882–889, 2013.

[14] S. X. Wu, J. Z. Fang, W. C. Xu, and C. Cen, "Hydrothermal synthesis, characterization of visible-light-driven α-Bi_2O_3 enhanced by Pr^{3+} doping," *Journal of Chemical Technology and Biotechnology*, 2013.

[15] H. Yu, R. Liu, X. Wang, P. Wang, and J. Yu, "Enhanced visible-light photocatalytic activity of Bi_2WO_6 nanoparticles by Ag_2O cocatalyst," *Applied Catalysis B*, vol. 111-112, pp. 326–333, 2012.

[16] J. Tang, Z. Zou, and J. Ye, "Efficient photocatalytic decomposition of organic contaminants over $CaBi_2O_4$ under visible-light irradiation," *Angewandte Chemie International Edition*, vol. 43, no. 34, pp. 4463–4466, 2004.

[17] P. Madhusudan, J.G. Yu, W. G. Wang, B. Cheng, and G. Liu, "Facile synthesis of novel hierarchical grapheme-$Bi_2O_2CO_3$ composites with enhanced photocatalytic performance under visible light," *Dalton Transactions*, vol. 41, no. 47, pp. 14345–14353, 2012.

[18] Q. Tian, J. Zhuang, J. Wang, L. Xie, and P. Liu, "Novel photocatalyst, $Bi_2Sn_2O_7$, for photooxidation of As(III) under visible-light irradiation," *Applied Catalysis A*, vol. 425-426, no. 28, pp. 74–78, 2012.

[19] L. Moens, P. Ruiz, B. Delmon, and M. Devillers, "Evaluation of the role played by bismuth molybdates in $Bi_2Sn_2O_7$±MoO_3 catalysts used for partial oxidation of isobutene to methacrolein," *Applied Catalysis A*, vol. 180, no. 1-2, pp. 299–315, 1999.

[20] H. Du, X. Yao, and L. Zhang, "Structure, IR spectra and dielectric properties of Bi_2O_3-ZnO-SnO_2-Nb_2O_5 quarternary pyrochlore," *Ceramics International*, vol. 28, no. 3, pp. 231–234, 2002.

[21] A. Walsh, G. W. Watson, D. J. Payne, G. Atkinson, and R. G. Egdell, "A theoretical and experimental study of the distorted pyrochlore $Bi_2Sn_2O_7$," *Journal of Materials Chemistry*, vol. 16, no. 34, pp. 3452–3458, 2006.

[22] C. A. Mims, A. J. Jacobson, R. B. Hall, and J. T. Lewandowski, "Methane oxidative coupling over nonstoichiometric bismuth-tin pyrochlore catalysts," *Journal of Catalysis*, vol. 153, no. 2, pp. 197–207, 1995.

[23] J. Wu, F. Huang, X. Lu, P. Chen, D. Wan, and F. Xu, "Improved visible-light photocatalysis of nano-$Bi_2Sn_2O_7$ with dispersed s-bands," *Journal of Materials Chemistry*, vol. 21, no. 11, pp. 3872–3876, 2011.

[24] Z. Liu, Z. Jian, J. Fang, X. Xu, X. Zhu, and S. Wu, "Low-temperature reverse microemulsion synthesis, characterization, and photocatalytic performance of nanocrystalline titanium dioxide," *International Journal of Photoenergy*, vol. 2012, Article ID 702503, 8 pages, 2012.

[25] W. Yin, W. Wang, L. Zhou, S. Sun, and L. Zhang, "CTAB-assisted synthesis of monoclinic $BiVO_4$ photocatalyst and its highly efficient degradation of organic dye under visible-light irradiation," *Journal of Hazardous Materials*, vol. 173, no. 1–3, pp. 194–199, 2010.

[26] S. Shen, L. Zhao, and L. Guo, "Cetyltrimethylammonium-bromide (CTAB)-assisted hydrothermal synthesis of $ZnIn_2S_4$ as an efficient visible-light-driven photocatalyst for hydrogen production," *International Journal of Hydrogen Energy*, vol. 33, no. 17, pp. 4501–4510, 2008.

[27] M. A. Subramanian, G. Aravamudan, and G. V. Subba Rao, "Oxide pyrochlores—a review," *Indian Academy of Sciences*, vol. 15, no. 2, pp. 55–143, 1983.

[28] P. Pascuta and E. Culea, "FTIR spectroscopic study of some bismuth germanate glasses containing gadolinium ions," *Materials Letters*, vol. 62, no. 25, pp. 4127–4129, 2008.

[29] Y. Wang, J. C. Shi, J. L. Cao, G. Sun, and Z. Y. Zhang, "Synthesis of Co_3O_4 nanoparticles via the CTAB-assisted method," *Materials Letters*, vol. 65, no. 2, pp. 222–224, 2011.

[30] M. Zhang, T. An, X. Hu, C. Wang, G. Sheng, and J. Fu, "Preparation and photocatalytic properties of a nanometer ZnO-SnO_2 coupled oxide," *Applied Catalysis A*, vol. 260, no. 2, pp. 215–222, 2004.

[31] A. Moral, M. D. Sicilia, S. Rubio, and D. Pérez-Bendito, "Determination of bisphenols in sewage based on supramolecular solid-phase extraction/liquid chromatography/fluorimetry," *Journal of Chromatography A*, vol. 1100, no. 1, pp. 8–14, 2005.

[32] Y. Huang, Q. Zhou, and G. Xie, "Development of micro-solid phase extraction with titanate nanotube array modified by cetyltrimethylammonium bromide for sensitive determination of polycyclic aromatic hydrocarbons from environmental water samples," *Journal of Hazardous Materials*, vol. 193, pp. 82–89, 2011.

[33] H. Niu, Y. Cai, Y. Shi, F. Wei, S. Mou, and G. Jiang, "Cetyltrimethylammonium bromide-coated titanate nanotubes for solid-phase extraction of phthalate esters from natural waters prior to high-performance liquid chromatography analysis," *Journal of Chromatography A*, vol. 1172, no. 2, pp. 113–120, 2007.

[34] S. I. Shah, W. Li, C. P. Huang, O. Jung, and C. Ni, "Study of Nd^{3+}, Pd^{2+}, Pt^{4+}, and Fe^{3+} dopant effect on photoreactivity of TiO_2 nanoparticles," *Proceedings of the National Academy of Sciences of the United States of America*, vol. 99, no. 2, pp. 6482–6486, 2002.